Control of chaotic spatiotemporal spiking by time-delay autosynchronization

G. Franceschini, S. Bose, and E. Schöll
Institut für Theoretische Physik, Technische Universität Berlin, Hardenbergstraße 36, D-10623 Berlin, Germany
(Received 7 April 1999)

A global time-delayed feedback control is applied to a globally coupled reaction-diffusion system describing charge transport in a bistable semiconductor. We demonstrate that a variety of spatiotemporal unstable periodic orbits (UPOs) embedded in a chaotic attractor of the spatially extended system can be stabilized using an extended time-delay autosynchronization algorithm. These UPOs correspond to spiking current filaments. We critically evaluate analytical approximations for the limits of control originally developed for low-dimensional temporal chaos and show that the delay time can be extrapolated with high accuracy, while the theoretical limit for the control of UPOs in terms of the product of the period and the largest Lyapunov exponent is not reached. If the global feedback is modified by a spatial filter, we achieve stabilization of different spatial patterns. [S1063-651X(99)07911-8]

PACS number(s): 05.45.−a, 05.70.Ln, 72.20.Ht

I. INTRODUCTION

During the last decade, the nonlinear dynamics of high-dimensional, spatially extended systems [1,2] on one hand, and the control of low-dimensional temporal chaos [3] on the other hand has stimulated a large amount of work. Only recently there have been attempts to combine these two issues and thus to extend the knowledge acquired in control of low-dimensional chaos to dynamic systems with a large number of degrees of freedom. The main difficulty arises from the fact that the standard control techniques [4–6] seem to work only for unstable periodic orbits with very few unstable directions. High dimensional systems exhibit spatiotemporal chaos yet do not normally have this property. Therefore, depending on the particular system under consideration, a variety of different approaches were proposed in the literature [7–12].

The interest in controlling chaos is due to the observation that small perturbations by external forces [4] or time-delayed feedback [5] can eliminate chaotic motion by stabilizing one of the unstable periodic orbits (UPO), which are embedded in any chaotic attractor. Analytical insight into the mechanism of delayed feedback control and the optimization of parameters [13–17] has only recently been achieved. While the control of electronic circuits [18,19], plasmas [20], optical [21–23], chemical [24], and biological [25,26] systems, for instance, has been widely studied, little work has been devoted to controlling current instabilities in semiconductors, although these systems would offer particularly useful applications if chaotic dynamics could be converted into a stable, tunable high-frequency electronic oscillator. Only purely temporal chaos control has been analyzed theoretically in the dynamic Hall effect [27] and in real-space transfer oscillators [28,29]. It is an aim of this work to fill this gap by demonstrating that chaotic spatiotemporal current density patterns in bistable semiconductor devices can be controlled by a time-delay autosynchronization method.

Charge transport in various semiconductor structures with bistable current-voltage characteristics can be modelled by a spatially extended reaction-diffusion system of activator-inhibitor type with global coupling [30],

$$\frac{d}{dt}u(t)=\alpha[(j_0-(u-\langle a\rangle)], \tag{1}$$

$$\frac{\partial a(x,t)}{\partial t}=f(a,u)+\frac{\partial^2 a}{\partial x^2}, \tag{2}$$

$$f(a,u)\equiv\frac{u-a}{(u-a)^2+1}-\mathcal{T}a.$$

Here $u(t)$ is the normalized voltage across the device and $a(x,t)$ is the activator variable which represents an internal degree of freedom like, e.g., a normalized interface charge density in the heterostructure hot-electron diode [30] or the voltage drop between the cathode and the *p*-base layer in a *pnpn* structure [37], and whose dynamics is governed by the nonlinear transport equation (2). The internal parameter $\mathcal{T}$ controls the size of the bistability range. The ratio of the timescales of the two variables u and a is determined by the parameter α, which is proportional to $1/(C_{int}+C_{ext})$, where C_{int} and C_{ext} are the internal and parallel external capacitances, respectively. Finally, j_0 is the driving current, which will be considered as bifurcation parameter. The normalized current density in the device is $j(x,t)=u(t)-a(x,t)$. The quantity $\langle a\rangle=\int_0^{L_x}a(x,t)\,dx$ in Eq. (1) denotes the spatial average of $a(x,t)$ over the transverse dimension L_x of the device (perpendicular to the current flow) and represents the global coupling due to the integrated current density. Thus Eq. (1) is Kirchhoff's circuit equation for the total current j_0 composed of the conduction current through the device $\langle j\rangle=u-\langle a\rangle$ and the capacitive currents. Throughout this paper we use dimensionless variables.

The spatially uniform fixed points of system (1) and (2) yield an *S*-shaped current-voltage characteristic $j_0(u)$, which is implicitly given by

$$u(j_0)=\frac{j_0}{\mathcal{T}(j_0^2+1)}+j_0. \tag{3}$$

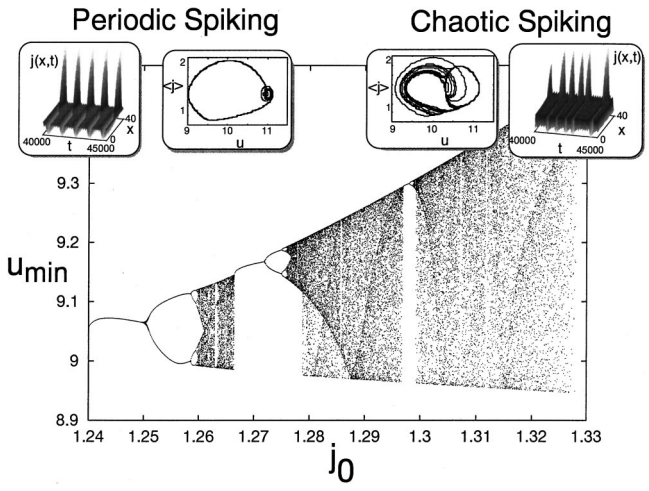

FIG. 1. Bifurcation diagram of spatiotemporal spiking of current filaments. The minima of the normalized voltage $u(t)$ with $u<10$ are plotted vs the control parameter j_0, which is the normalized driving current. The insets show the spatiotemporal evolution of the current density $j(x,t)=u(t)-a(x,t)$ and the $(u,\langle j\rangle)$ phase portrait of periodic ($j_0=1.245$) and chaotic spiking ($j_0=1.31$). Other parameters: $L_x=40$, $\alpha=0.035$, $\mathcal{T}=0.05$. All quantities are dimensionless.

It describes bistability between a high-conductivity and a low-conductivity state in a certain range of voltages u. It is well known that this bistability can give rise to the bifurcation of spatially inhomogeneous current density distributions in the form of *current filaments* [31,32], i.e., the cross section of the current flow exhibits a region of high current density embedded in a low-conductivity phase. Higher bifurcations have been found to lead to complex spatiotemporal dynamics of these current filaments [33,34] and in particular, the system (1) and (2) displays periodic and chaotic sequences of *spatiotemporal spiking* of the current density $j(x,t)$ [30,35,36]. This is in good agreement with experiments in Si *pnpn* diodes [37] and other layered semiconductor structures with *S*-shaped current-voltage characteristics [38].

Figure 1 shows a typical bifurcation diagram of spiking filaments for $\alpha=0.035$ and $\mathcal{T}=0.05$. The minima of the voltage drop across the device $u(t)$ are plotted versus the driving current as the bifurcation parameter. Period-doubling sequences and alternating bands of chaotic and periodic spiking can clearly be seen. The insets depict the spatiotemporal dynamics of the current density $j(x,t)$ and the corresponding orbits in the $(u,\langle j\rangle)$ phase plane for a typical operating point in the periodic ($j_0=1.24$) and the chaotic ($j_0=1.31$) regime.

It is the purpose of this paper to extend methods of time delayed feedback control which have been developed for low-dimensional systems, viz. ordinary differential equations [5] and iterated maps [6], to the chaotic spatiotemporal spiking attractor of the globally coupled reaction-diffusion system introduced above. We shall demonstrate that by applying an appropriate global feedback the UPOs corresponding to spatio-temporal spiking can be stabilized. It should be noted that although our system of partial differential equations has infinitely many degrees of freedom, it possesses a low-dimensional chaotic attractor [36].

The organization of the paper is as follows. After this introduction, we shall apply the method of extended time delay autosynchronization to stabilize spatiotemporal UPOs (Sec. II). In Sec. III an analytical approach [13] will be used to optimize the parameters that are given by the delay time τ and the strength K of the control feedback signal. In Sec. IV we analyze the bifurcations that occur at the boundaries of the control domain as a function of K. In Sec. V we touch the issue of spatial filtering. Finally, we conclude by discussing the limits of control.

II. STABILIZATION OF UNSTABLE PERIODIC ORBITS

In order to stabilize UPOs of the chaotic dynamic systems (1) and (2) we shall employ a continuous feedback as suggested by Pyragas [5] for ordinary differential systems to synchronize the current state of the system with a time-delayed version of itself (''time-delay autosynchronization,'' TDAS). However, for the distributed system (1) and (2) we have not been able to obtain chaos control by simply applying this feedback to the temporal variable u. Rather, the most efficient control of the spatiotemporal dynamics is achieved when the spatially averaged variable $a(x,t)$ is used for the construction of the control signal $\epsilon(t)$ and when this signal is fed back into the same spatiotemporal variable $a(x,t)$, i.e., if Eq. (2) is replaced by

$$\frac{\partial a(x,t)}{\partial t}=f(a,u)+\frac{\partial^2 a}{\partial x^2}+\epsilon(t),$$
$$\epsilon(t)\equiv K\,[\langle a\rangle(t-\tau)-\langle a\rangle(t)]\equiv K\xi(t), \tag{4}$$

where K is the control amplitude, and τ is the delay time. Note that the feedback is a spatially homogeneous signal that applies the same perturbation to every point of the distributed system. Nevertheless it turns out that it is capable of stabilizing the extremely inhomogeneous spatiotemporal spikes representing the UPOs of the system. Physically, it may be realized by an external control circuit using a lateral gate electrode located at the active layer. Since the dimensionless control variable $\langle a\rangle=u-\langle j\rangle$ is given in terms of the voltage drop u and the integral current $\langle j\rangle$ through the device, i.e., electrical quantities that are easily accessible experimentally, it is straightforward to implement a control circuit which couples the delayed difference $\epsilon(t)$ back to the lateral gate potential. If this gate electrode is extended in the x direction and imposes the same electrical input along the whole gate, a global coupling to the distributed variable $a(x,t)$ is realized. A concrete setup of such a distributed lateral gate structure has been described for a gate-driven *pnpn* thyristor device [39,40], and the dynamic equation for the *p*-base potential a including its dependence upon the gate-potential has been derived. (Note that the global couplings due to external circuits are used there in a different context, i.e., for control of the propagation of lateral current density fronts.) Similar lateral gate configurations have also been realized experimentally in mesa-etched resonant tunneling semiconductor structures where the charge density in the active quantum well layer corresponding to the internal variable a can be readily controlled by tuning the gate potential.

A natural extension of the Pyragas scheme is given by a feedback that takes into account several previous states and

for which the term ''extended time-delay autosynchronization'' (ETDAS) was proposed [6]. Using this extension we obtain the control signal

$$\epsilon(t)=K\left((1-R)\sum_{m=1}^{\infty}R^{m-1}\langle a\rangle(t-m\tau)-\langle a\rangle(t)\right)$$
$$\equiv K\xi(t) \quad 0\leqslant R<1, \tag{5}$$

where R controls the contributions of previous states; small values of R indicate a short time memory, while larger values give a stronger weight to all previous states. With increasing R orbits of higher order and orbits with larger Lyapunov exponents are likely to be stabilized [41,16]. The case $R=0$ corresponds to the simple TDAS scheme.

In our computer simulations we choose as initial conditions the unstable state corresponding to the middle branch of the S-shaped current-voltage characteristic perturbed by small inhomogeneous random fluctuations $[\delta a(x),\delta u]$ of less than 1%. The bifurcation parameter j_0 is chosen in the regime of chaotic spiking (cf. Fig. 1). The initial condition thus falls within the basin of the chaotic spiking attractor. We use a forward Euler algorithm with a spatial discretization in 25 grid points.

Figure 2 shows the stabilization of such a chaotic spiking mode and elucidates the dynamics of the uncontrolled [Fig. 2(a)] and the controlled system [Fig. 2(b)] by comparing the phase portraits of the attractor projected onto the $(u,\langle j\rangle)$ phase plane, the power spectra of the voltage $u(t)$, and the spatiotemporal distribution of the current density $j(x,t)$. The simulations were performed for 10^5 time units. The data of the last 2×10^4 time units were used to plot the phase portrait and to compute the power spectrum. Figure 2(a) illustrates the embedding of the UPO in the chaotic attractor by showing the phase portrait of both the controlled UPO (thick curve) and the uncontrolled system. The delay time is equal to the period of the stabilized periodic orbit. The large loop in the phase plane corresponds to the localized spike of the current density $j(x,t)$ while the smaller loop reflects the uniform small-amplitude relaxation oscillation in between two spikes; note that altogether it represents a period-one orbit. We have used a slightly modified ETDAS algorithm by truncating the series in Eq. (5) for $m>N$; the memory thus comprises the N previous states at times $t-\tau,t-2\tau,\ldots,t-N\tau$, and neglects further states in the past. N is chosen such that R^N is smaller than 10^{-6}. Thus with increasing R more previous states have to be taken into account.

Figures 2(c) and 2(d) show the time series of the control signal $\epsilon(t)$ and the dynamic variable $u(t)$. Control is switched on at $t=7000$. After about 20 UPO periods the control signal vanishes and the chaotic oscillations of $u(t)$ become periodic.

Stabilization of periods of higher order is shown in Fig. 3. For a fixed bifurcation parameter j_0 the unstable period-one, period-two, and period-four orbits can be stabilized with a subsequently increasing memory amplitude R. We have been able to achieve control of the period-1 orbit with $R=0$, while higher orbits (>2) require $R\neq0$. In Figs. 3(b) and 3(c) the additional frequency peaks at 1/2 and 1/4 of the fundamental frequency can be seen in the power spectra, especially in the higher harmonics. Denoting the periods of the controlled

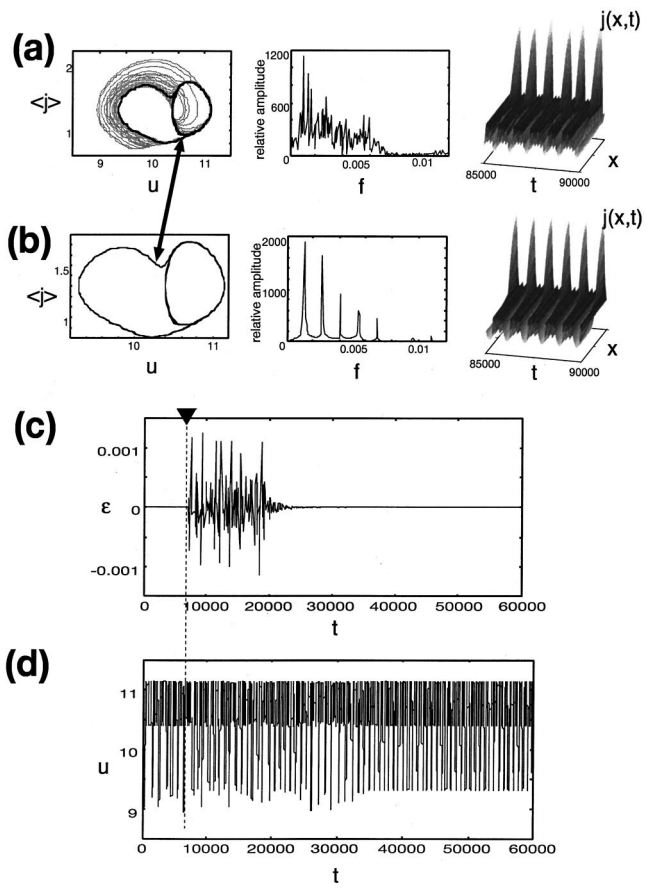

FIG. 2. Phase portrait of the attractor in the $(u,\langle j\rangle)$ phase plane, power spectrum of $u(t)$, and spatiotemporal distribution of the current density $j(x,t)$ for (a) the uncontrolled and for (b) the controlled system. The thick trajectory in the phase portrait of the chaotic attractor in (a) represents the controlled UPO from (b). (c) and (d) show the control signal $\epsilon(t)$ and the voltage $u(t)$ vs time, respectively. Control is switched on at $t=7000$. Parameters: $j_0=1.302$, $\tau=732.4$, $K=0.000\,548$, $R=0.2$, $N=8$. The other numerical parameters are as in Fig. 1.

UPO by τ_1, τ_2, and τ_4, respectively, we find that the periods of higher order τ_2 and τ_4 are not exact integer multiples of τ_1, but there is a discrepancy of about 1% between $n\tau_1$ and τ_n. This deviation is significant since control fails for $\tau_2=2\tau_1$ or $\tau_4=4\tau_1$ however one adjusts the coupling constant K.

III. OPTIMIZATION OF CONTROL PARAMETERS

By continuous variation of τ and K and simultaneous monitoring of the control signal $\epsilon(t)=K\xi(t)$ the control parameters τ and K can be adjusted to their optimal values [5]. A satisfactory stabilization is achieved when the control signal becomes negligibly small after some transient time. Therefore, we compute the temporally averaged asymptotic control signal $\langle|\xi|\rangle_t$ for each simulation. We proceed according to the following steps. First, the delay time τ is varied for a fixed value of the estimated control amplitude K. If K is chosen in the right order of magnitude, $\langle|\xi|\rangle_t$ as a function of τ exhibits sharp resonant minima as depicted in Fig. 4; the positions of the minima indicate the unknown periods T_i of the UPOs [5]. Next, τ is fixed to one of these UPO reso-

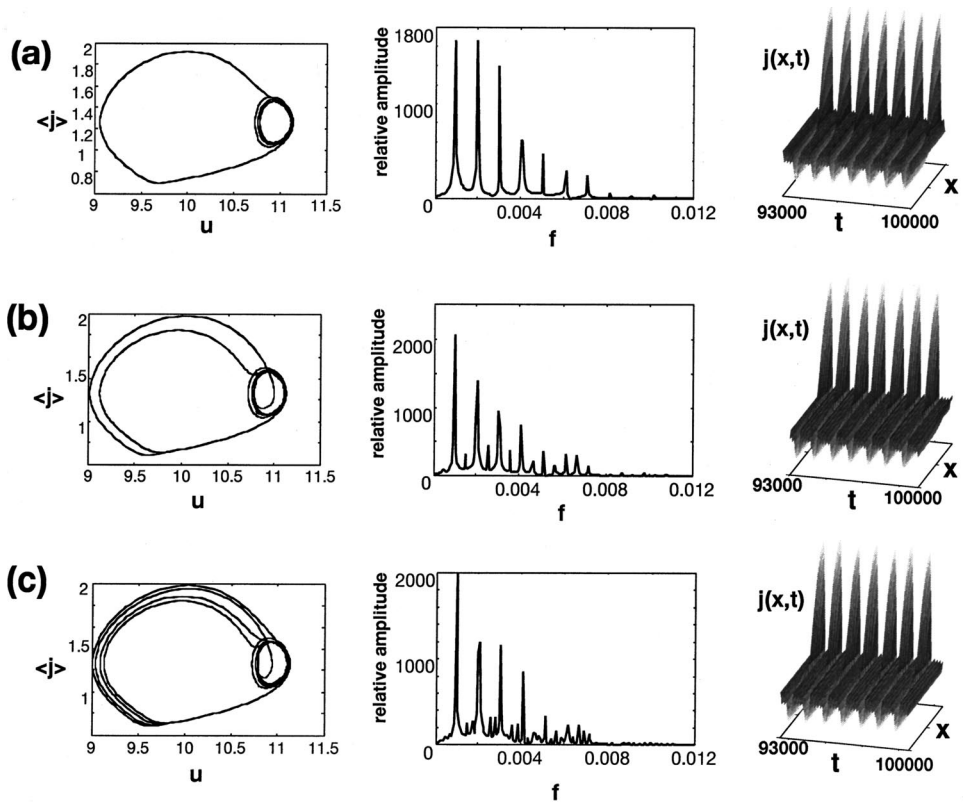

FIG. 3. Stabilized periodic attractors in the $(u,\langle j\rangle)$ phase plane, power spectrum of $u(t)$, and spatiotemporal distribution of the current density $j(x,t)$ for the controlled system with the bifurcation parameter $j_0=1.262$: (a) period-1, (b) period-2, and (c) period-4 orbit. Control parameters: (a) TDAS: $\tau=985.9$, $K=0.000\,513$, (b) ETDAS: $\tau=1949.2$, $K=0.000\,312$, $R=0.1$, $N=6$, (c) ETDAS: $\tau=3909.5$, $K=0.000\,288$, $R=0.2$, $N=10$. The other numerical parameters are as in Fig. 1.

nances, and K is optimized. Generally, the control signal vanishes in a finite control domain of K-values (Fig. 5). In Fig. 5 we have also plotted the largest nonzero Lyapunov exponent λ which is positive for the uncontrolled chaotic attractor ($K=0$) and negative in case of successful stabilization of the UPO. An optimum value of K is indicated by a minimum Lyapunov exponent. Note, however, that a negative Lyapunov exponent alone is not sufficient for successful control of a UPO since it might also be due to an artificially induced limit cycle which exists only with a nonvanishing control signal as, e.g., shown in Fig. 5 for the K-range above K_{max}. It is the result of unintentional synchronization of the system with the control signal giving rise to a limit cycle of period $\Theta\neq\tau$ that is not a UPO of the chaotic attractor.

By iterating the procedure described above an optimal choice of both τ and K can be obtained although this may be quite cumbersome due to the extremely sharp resonances in τ. Empirical schemes to improve the estimate of the delay time by a self-adaptive control have been suggested for special cases [42]. A very promising technique to extrapolate the unknown UPO period T on the basis of repeated application of an analytical approximation formula was recently proposed for chaos control in ordinary differential equations by Just *et al.* [14]. If the delay time τ and the UPO period T do not coincide the system responds with a periodic signal of period Θ for not too large delay mismatch. An expansion in terms of the delay mismatch $\tau-T$ yields

$$\Theta(K,\tau)=T+\frac{K}{K-\kappa}(\tau-T)+\mathcal{O}((\tau-T)^2). \qquad (6)$$

Θ depends on the control parameters K,τ and on a system parameter κ and obeys the constraint $\Theta(K,\tau=T)=T$. The parameter κ comprises all details about the coupling of the control force and is unknown, as is the UPO period T. It is therefore sufficient to determine Θ for two sets of parameters K,τ. Then T and κ can be computed from the system of two nonlinear Eqs. (6) using Newton's method. In the next iteration we use the computed approximation of T as new delay τ in the subsequent simulation. Again we expect the system to synchronize with a new period Θ. Using this set of data and the better of the two initial guesses we can again solve the system (6) and thus obtain a better approximation of T. The algorithm therefore opens up the possibility of a recursive approximation of the unknown UPO period T. We have applied the above procedure to our system exhibiting spatiotemporal chaos. For the bifurcation parameter $j_0=1.262$ (cf. Figs. 4 and 5), $K=0.0006$ and initial guesses of the unknown period $\tau_1^{(0)}=500$ and $\tau_2^{(0)}=1200$ we have determined Θ and numerically solved Eq. (6) for $T^{(1)}$. After only

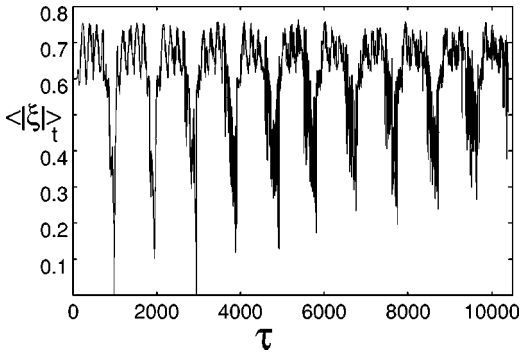

FIG. 4. Mean asymptotic control signal $\langle|\xi|\rangle_t$ as a function of the delay time τ for $j_0=1.262$ and fixed $K=0.000\,479$ (TDAS). For each value of τ the control signal $|\xi|$ has been averaged over the last 20 000 time steps of a simulation of 2×10^5 time units. The other numerical parameters are as in Fig. 1.

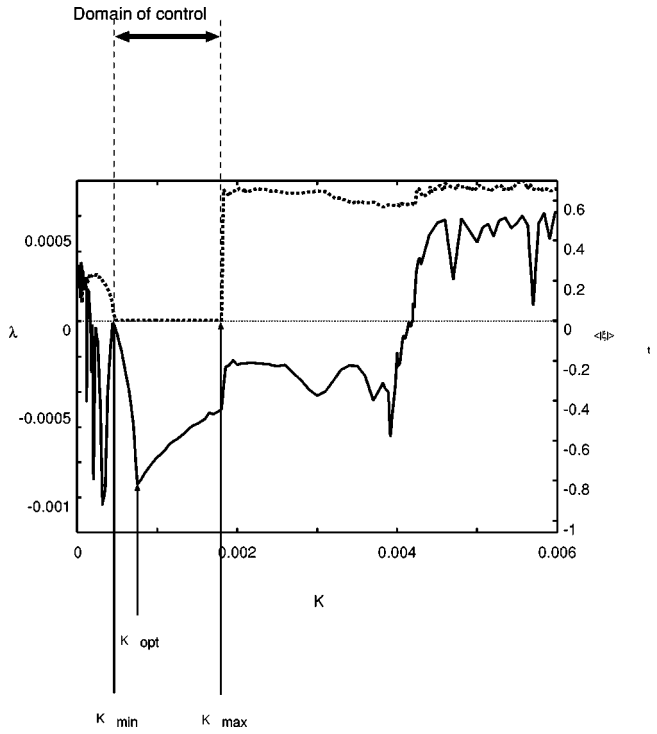

FIG. 5. Largest nonzero Lyapunov exponent λ (solid line) and mean asymptotic control signal $\langle|\xi|\rangle_t$ (dotted line) as a function of the control amplitude K for $j_0=1.262$ and fixed $\tau=985.9$ (TDAS). Optimal control (K_{opt}) is achieved when the control signal vanishes and $\lambda(K)$ reaches its minimum. K_{min} and K_{max} mark the boundaries of the domain of control. For each value of K the control signal $|\xi|$ has been averaged over the last 20 000 time steps of a simulation of 2×10^5 time units. The other numerical parameters are as in Fig. 1.

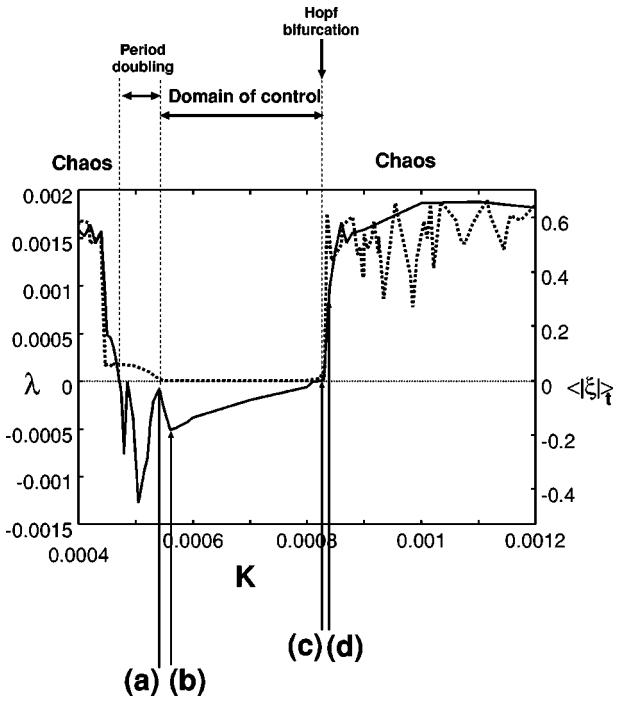

FIG. 6. Same as Fig. 5 for $j_0=1.302$, $\tau=732.4$, $R=0.2$, $N=8$. The following values of K are marked: (a) Period doubling bifurcation (flip instability), (b) optimal UPO control, (c) Hopf instability (torus), (d) onset of chaos. For each value of K the control signal $|\xi|$ has been averaged over the last 20 000 time steps of a simulation of 2×10^5 time units.

four simulations with different values of τ and three iterations of Eq. (6) we obtain the UPO period $T^{(3)}\approx983.2$. In spite of the large initial delay mismatch this result is in excellent agreement with the true UPO period $T=985.9$ (the relative deviation is less than 0.3%) and is reproducible for even worse initial guesses and other values of j_0. This indicates that the algorithm is very robust and efficient not only for purely temporal chaos but also for high-dimensional systems.

IV. BIFURCATIONS AT THE BOUNDARY OF THE DOMAIN OF CONTROL

Once we have adjusted the delay time τ to the UPO period T we can vary the control amplitude K in a whole interval (K_{min},K_{max}) and still achieve control of the UPO. This domain of control is characterized by a vanishing control signal (and thus by $\langle|\xi|\rangle_t=0$) and by a negative Lyapunov exponent $\lambda(K)$ (Fig. 5). At the lower boundary of this K-domain the stabilized orbit decays via a period doubling bifurcation (''flip instability'' corresponding to a torsion of nearby orbits by π during one cycle) while at the upper boundary a Hopf bifurcation occurs [16,15]. The Hopf bifurcation adds an incommensurate frequency to the stabilized UPO limit cycle and thus gives rise to a two-torus preceding the onset of chaos via quasiperiodicity.

Figure 6 presents an overview of the bifurcations with respect to K. For small values of K we find chaotic behavior characterized by a positive Lyapunov exponent and a nonvanishing control signal, as expected for too weak control. As we increase K, an inverse period doubling cascade sets in which finally leads to the stabilized UPO in the domain of control [point (a)]. At each period doubling bifurcation the Lyapunov exponent vanishes [43]. In the period doubling regime the control signal remains positive. Within the domain of control optimal stabilization is achieved at $K=K_{opt}$, where the negative Lyapunov exponent $\lambda(K)$ is minimum [point (b)]. Further increase of K leads to a Hopf bifurcation associated with a rise of the control signal $\langle|\xi|\rangle_t$ to slightly positive values at the upper boundary of the control domain [point (c)] followed by a sharp increase as chaos sets on [point (d)]. The Lyapunov exponent λ becomes zero at the Hopf bifurcation as a signature of the two-torus, which possesses two vanishing Lyapunov exponents (note that a second Lyapunov exponent is zero throughout the whole range of K), and jumps to positive values only as chaos occurs. For very large control amplitude the controlled variable a is driven too hard and decouples from the other variable, therefore the control of UPOs fails.

Figure 7 presents simulations for the points (a)–(d) of Fig. 6. Figures 7(a) and 7(c) correspond approximately to the respective bifurcation points, while Fig. 7(b) represents the stabilized reference UPO at $K=K_{opt}$, and Fig. 7(d) shows the onset of chaos just above the Hopf bifurcation. The power spectra in Figs. 7(a) and 7(c) clearly reveal the appearance of the subharmonic frequency and the higher incommensurate frequency associated with period doubling and Hopf bifurcation, respectively (marked by arrows). The

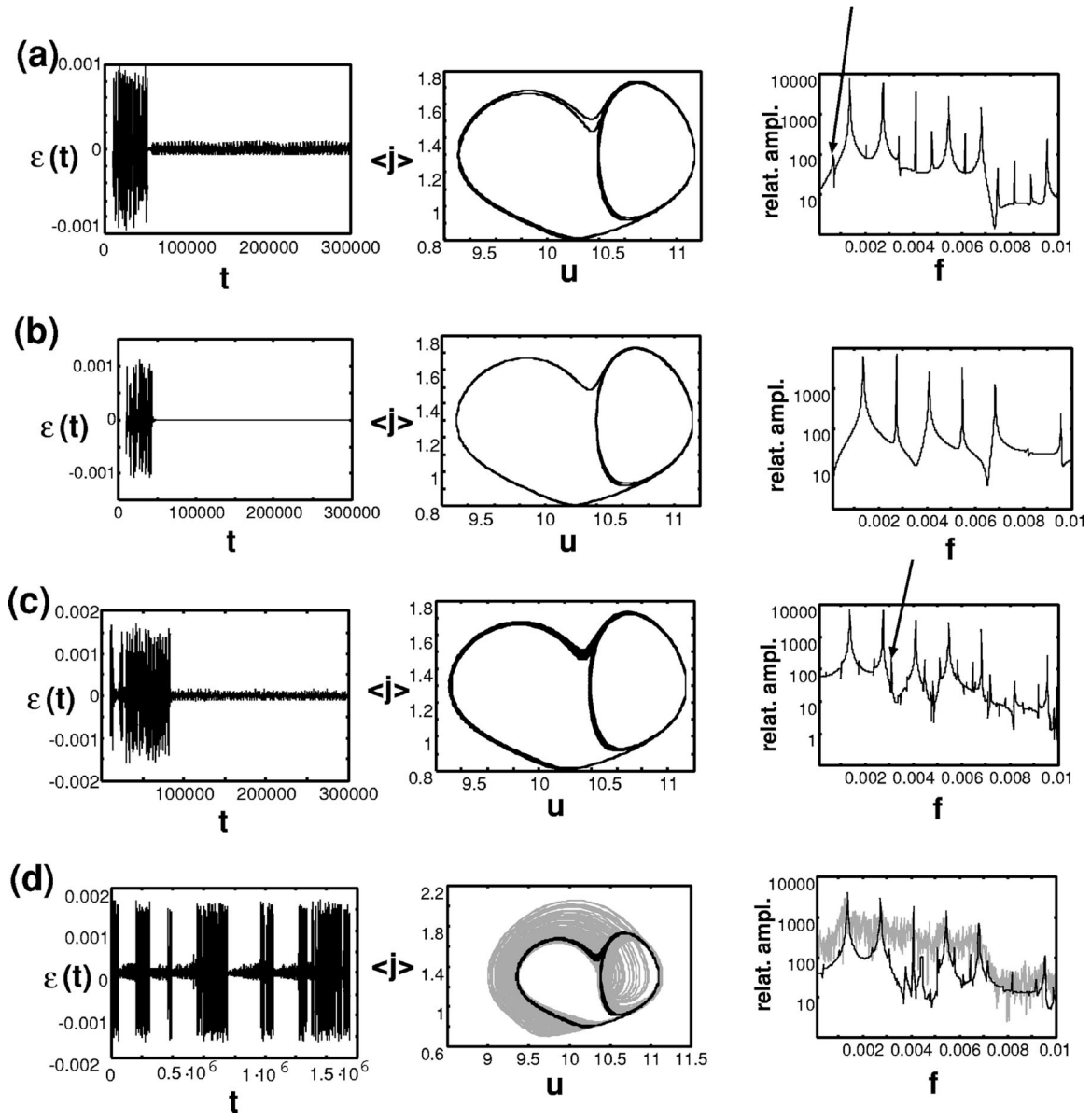

FIG. 7. Control signal $\epsilon(t)$, phase portraits $(u,\langle j\rangle)$, and power spectrum of $u(t)$ for different values of the control amplitude K marked in Fig. 6. (a) Period-doubling (flip instability) at the lower boundary of the control regime, (b) reference UPO at optimum $K=K_{opt}$, (c) Hopf instability at the upper boundary of the control regime, (d) onset of chaos beyond the Hopf bifurcation via intermittency: quasiperiodic (black lines) and chaotic (gray lines) spiking oscillations alternate. The arrows in (a) and (c) indicate the additional frequencies with respect to (b). Parameters: $j_0=1.302$, $\tau=732.4$, $R=0.2$, $N=8$, (a) $K=0.000\,54$, (b) $K=0.000\,56$, (c) $K=0.000\,834$, (d) $K=0.000\,838$.

onset of chaos in Fig. 7(d) shows intermittent behavior where the dynamics seems to oscillate between the two-torus and the chaotic attractor. Both dynamic states are plotted separately in the phase portrait and in the power spectrum.

For different parameters j_0 we have also observed more complex bifurcation scenarios. In Fig. 5, e.g., the Hopf bifurcation is concealed by a regime where a synchronized limit cycle (negative Lyapunov exponent) is enforced by the control ($\langle|\xi|\rangle_t\neq 0$). A closer inspection shows that at least in some range of $K>K_{max}$ bistability between the forced limit cycle and a controlled UPO occurs, depending upon the initial conditions. This can be understood by noting that the basin of attraction of the controlled UPO becomes smaller as the boundaries of the control domain are approached.

V. PATTERN SELECTION BY SPATIAL FILTERING

Up to now we have only considered a spatially homogeneous feedback $\epsilon(t)$ at every point of the distributed system. The idea of using a spatially inhomogeneous feedback arises from the observation that in the uncontrolled system there exist various locally stable or even unstable spatially inhomogeneous modes, e.g., spiking current filaments located in the center of the sample, but these are only observed for special initial conditions. Note that in the absence of control a random initial distribution always gives rise to a (spiking) filament, which is pinned to the boundary [cf., e.g., Fig. 8(a)]; this dominant spatial mode results from the attraction exerted upon filaments by Neumann boundary conditions [44]. By tailoring appropriate spatiotemporal control signals

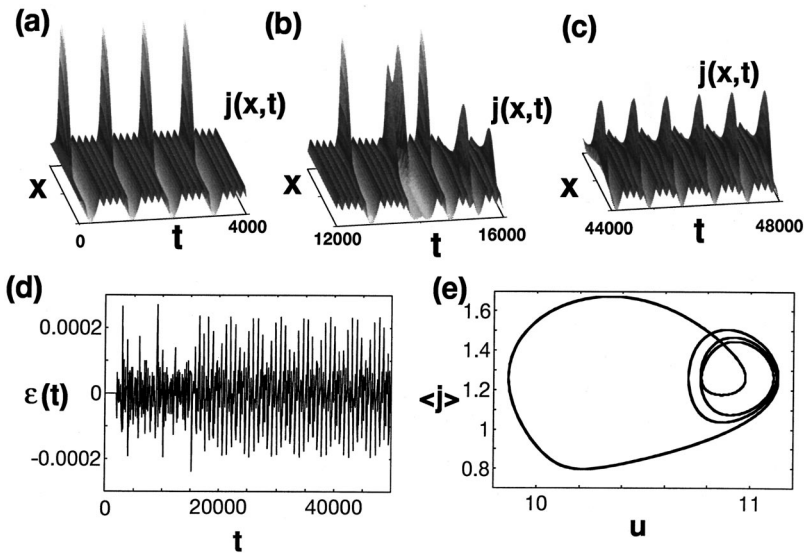

FIG. 8. Suppression of the dominant spatial mode in favor of an unstable one by spatial filtering. In (a)–(c) the spatiotemporal distribution of the current density $j(x,t)$ is plotted for different time regimes. (a) Asymmetric spiking filament at the boundary, induced by random initial conditions. (b) Transient regime of coexistence of both spiking modes after control is switched on at $t=2000$. (c) Symmetric spiking mode prevails over the asymmetric one and forms the asymptotic pattern. (d) Control signal $\epsilon(t)$, (e) phase portrait of the stabilized limit cycle corresponding to (c). Parameters: $j_0=1.262$, $K=0.0002$, $R=0$, $\tau=985.5$, asymptotic period of the response signal $\Theta=778.3$. The other numerical parameters are as in Fig. 1.

$\epsilon(x,t)$ which resemble the spatial profile of the desired modes one can expect to stabilize some of them from random initial conditions. Thus, chaos control in spatiotemporal systems could be used for pattern selection that opens up promising applications as distributed semiconductor memory devices and neural networks.

We illustrate this idea for a spatial mode $j(x,t)$ whose profile is symmetric and exhibits a peak (spike) at the center of the sample. This mode is unstable and can only be observed if the initial distribution of $j(x,t)$ is perfectly symmetric and the system is noise-free. In order to stabilize this symmetric spiking mode we apply a spatially modulated control signal $\epsilon_{inhom}(x,t)$, which favors the considered symmetry and can be constructed from the homogeneous control signal $\epsilon(t)$ in the following way:

$$\epsilon_{inhom}(x,t)=\epsilon(t)\left[1-\frac{1}{2}\cos\left(\frac{2\pi}{L_x}x\right)\right]$$
$$\epsilon(t)\equiv K[\langle a\rangle(t-\tau)-\langle a\rangle(t)]. \tag{7}$$

Figure 8 shows the results of a simulation with this spatially inhomogeneous feedback control. For random initial conditions the dominant spatial mode is always given by a chaotically spiking profile $j(x,t)$ with the spike located at the boundary [Fig. 8(a)]. After control is switched on, there is a transition period in which the dominant mode (favored by the boundary conditions) coexists with the symmetric mode (favored by the control signal) [Fig. 8(b)]. Finally the symmetric mode wins and the corresponding orbit is stabilized asymptotically [Fig. 8(c)]. The phase portrait in Fig. 8(e) suggests that the controlled orbit is periodic though not a UPO of the chaotic attractor since the control signal $\epsilon(t)$ does not vanish after some transient time [Fig. 8(d)]. Thus, the period of the stabilized limit cycle Θ does not coincide with the delay time τ. Nevertheless, we stress that by means of a weak perturbation we have succeeded in suppressing the dominant *spatial* mode in favor of an unstable one and to replace the *temporally* chaotic sequence of spikes by a periodic sequence.

VI. DISCUSSION

A rough estimate of the efficiency of the ETDAS scheme for temporal chaos in ordinary differential equations has been given by Just [16,15]: Only those UPOs can be stabilized that obey the constraint

$$\lambda\tau\leqslant 2\,\frac{1+R}{1-R}. \tag{8}$$

Thus, the simple TDAS scheme ($R=0$) is expected to be able to stabilize UPOs whose product of the Lyapunov exponent λ and the period τ does not exceed 2. In practice we have been able to control UPOs in our spatially extended system with global feedback only for lower values.

Empirically we found that both TDAS and ETDAS work successfully for UPOs with $\lambda\tau\lesssim 1.2$. If on the other hand $\lambda\tau>1.2$, the TDAS scheme starts to fail while ETDAS still works successfully if the Lyapunov exponent of the uncontrolled system is not too large. The best results we obtained were the stabilization of a high period UPO with a small Lyapunov exponent for $j_0=1.262$ ($\lambda=4.8\times10^{-4}$, $\tau=3909.5$ and thus $\lambda\tau\approx 1.9$) and of a highly unstable UPO for $j_0=1.305$ ($\lambda=2.58\times10^{-3}$, $\tau=730.3$, $\lambda\tau\approx 1.9$). Both orbits could only be controlled with ETDAS.

In parameter regions where the largest Lyapunov exponent is greater than 2.4×10^{-3} (i.e., $1.309\leqslant j_0\leqslant 1.314$) we have not been able to stabilize any UPO at all, although we extrapolate periods of the order of $\tau\approx 700$, and (if the Lyapunov exponent of the UPO and of the uncontrolled system do not differ significantly) $\lambda\tau<2$ would still hold. This could possibly be improved by making use of a technique developed by Zoldi to calculate UPOs explicitly using a damped-Newton method [45]. We suggest that it might be possible to stabilize some of these UPOs by means of more sophisticated control techniques, e.g., with a spatially filtered control signal.

Figure 9 summarizes our empirical findings for different values of λ and τ by showing the domains of control in the diagram of $\langle|\xi|\rangle_t$ as a function of K for different ETDAS realizations. The control domain comprises all values of K for which $\langle|\xi|\rangle_t$ vanishes. In Fig. 9(a), e.g., we have λ

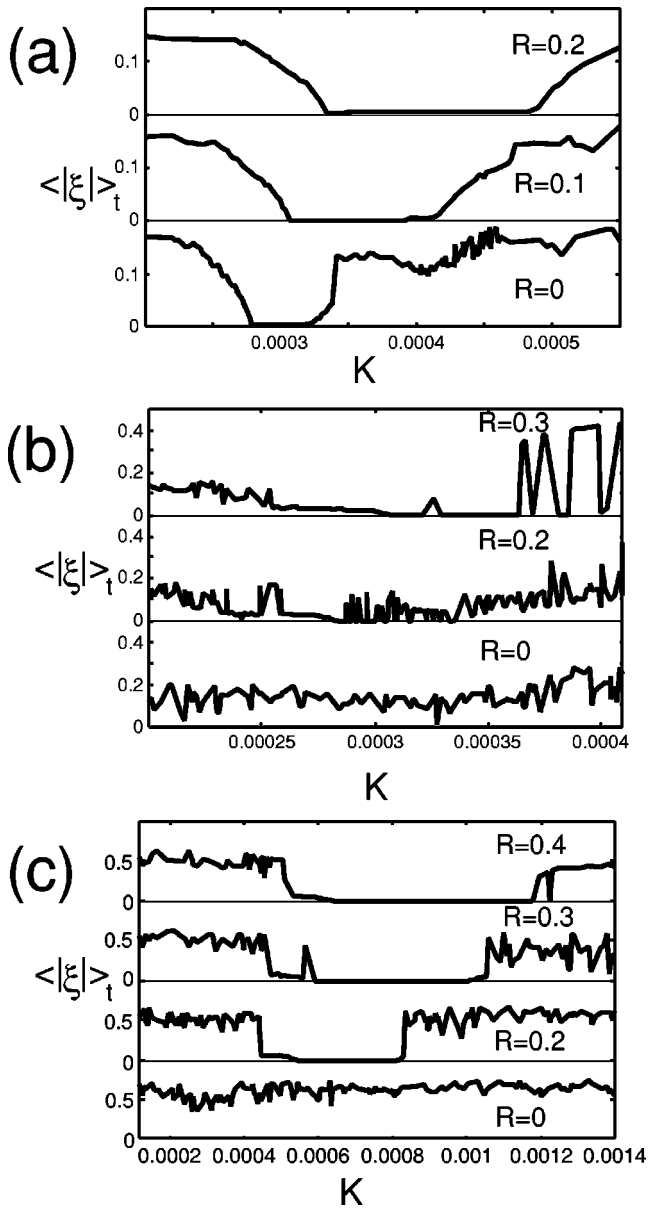

FIG. 9. Domains of control for different values of $\lambda\tau$ and R. UPO stabilization is achieved if the mean control signal $\langle|\xi|\rangle_t$ vanishes in some interval of K. (a) $j_0=1.262$, $\tau=1949.9$ (period-2), $\lambda\tau\approx1.2$. (b) $j_0=1.262$, $\tau=3909.5$ (period-4), $\lambda\tau\approx1.9$ (c) $j_0=1.302$, $\tau=732.4$ (period-1), $\lambda\tau\approx1.4$. For each value of K the control signal $|\xi|$ has been averaged over the last 20 000 time steps of a simulation of 2×10^5 time units. The other numerical parameters are as in Fig. 1.

$=6.2\times10^{-4}$, $\tau=1949.2$ for the period-2 UPO, and thus $\lambda\tau\approx1.2$. For this uncritical value of $\lambda\tau$ both the TDAS ($R=0$) and the ETDAS ($R>0$) scheme work in a finite K-interval, as is evident from the vanishing control signal. It should be noted that with increasing R the control domain is shifted to larger values of K and becomes wider, in good agreement with the theoretical predictions for temporal chaos [16]. For the period-4 UPO at the same value of j_0 [Fig. 9(b)] $\lambda\tau\approx1.9$, and control has no longer been achieved by the TDAS scheme ($R=0$), while the ETDAS scheme with $R>0$ still works, although large fluctuations in $\langle|\xi|\rangle_t$ are present. They are a result of the shrinking attractor basin which prevents stabilization for some realizations of the random initial conditions, even though for $R=0.2$, e.g., the theoretical limit of $\lambda\tau=3$ is by far not reached. In Fig. 9(c) we consider a UPO with $\lambda\tau\approx1.4$ for a different bifurcation parameter j_0; here the Lyapunov exponent is larger ($\lambda=1.88\times10^{-3}$) and the simple TDAS scheme does not allow stabilization even of the period-1 UPO. On the other hand there is still a large control domain for the feedback schemes with longer memory ($R>0$), and the small shift of the lower stability boundary (flip instability) and the stronger shift of the upper stability boundary (Hopf instability) with increasing R agrees well with the theoretical predictions [16].

In conclusion, we have been able to demonstrate that a variety of spatiotemporal UPOs embedded in a chaotic attractor of a distributed system can be stabilized using an extended time-delay autosynchronization algorithm. These UPOs correspond to spiking current filaments. We have critically evaluated numerical techniques and analytical approximations originally developed for *temporal* chaos [14,16] and found that a number of properties of chaos control in low-dimensional temporal systems carry over to the *spatiotemporally* chaotic reaction-diffusion system. We have confirmed that the delay time of global time-delayed feedback control (which is adjusted to the UPO period T) can be extrapolated with high accuracy from the periodic response of the system. We have also gained insight into the mechanism of spatiotemporal chaos control by analyzing the bifurcations at the boundaries of the control domain. While the gross features agree with the case of temporal chaos, we have found a higher sensitivity to noise which appears to be due to smaller attractor basins and multistability of the spatiotemporal patterns associated with the larger number of degrees of freedom. The theoretical limit for the control of temporal UPOs, which is given by $\lambda\tau\leqslant2$ for the Pyragas feedback, and by $\lambda\tau\leqslant2(1+R)/(1-R)$ for the extended time-delay autosynchronization scheme, has not been reached in our simulations. Further analytical and numerical work is necessary to explore the limits of control for spatiotemporal systems. Nevertheless, the ETDAS scheme represents a significant improvement of the simple Pyragas feedback. If the global feedback is modified by a spatial filter, we can achieve pattern selection and stabilization of otherwise unstable spatial modes corresponding to different locations of the spikes within the sample.

Our findings offer promising potential applications since the feedback can be readily realized for our distributed bistable semiconductor system by gate control circuits. Thus, it should be possible to build stable, tunable microwave oscillators on that principle.

ACKNOWLEDGMENTS

We are grateful to S. Zoldi, W. Just, and J.C. Claussen for enlightening discussions. This work was partially supported by the DFG in the framework of SFB 555.

[1] A. S. Mikhailov, *Foundations of Synergetics 1*, 2nd ed. (Springer, Berlin, 1994).
[2] F. Busse and S. Müller, *Evolution of Spontaneous Structures in Dissipative Continuous Systems* (Springer, Berlin, 1998).
[3] H. G. Schuster, *Handbook of Chaos Control* (Wiley-VCH, Weinheim, 1999).
[4] E. Ott, C. Grebogi, and J. A. Yorke, Phys. Rev. Lett. **64**, 1196 (1990).
[5] K. Pyragas, Phys. Lett. A **170**, 421 (1992).
[6] J. E. S. Socolar, D. W. Sukow, and D. J. Gauthier, Phys. Rev. E **50**, 3245 (1994).
[7] V. Petrov, M. J. Crowley, and K. Showalter, Phys. Rev. Lett. **72**, 2955 (1994).
[8] D. Battogtokh and A. Mikhailov, Physica D **90**, 84 (1996).
[9] M. Ding, W. Yang, V. In, W. L. Ditto, M. L. Spano, and B. Gluckman, Phys. Rev. E **53**, 4334 (1996).
[10] M. E. Bleich, D. Hochheiser, J. V. Moloney, and J. E. S. Socolar, Phys. Rev. E **55**, 2119 (1997).
[11] M. Münkel, F. Kaiser, and O. Hess, Phys. Rev. E **56**, 3868 (1997).
[12] R. O. Grigoriev, M. C. Cross, and H. G. Schuster, Phys. Rev. Lett. **79**, 2795 (1997).
[13] W. Just, T. Bernard, M. Ostheimer, E. Reibold, and H. Benner, Phys. Rev. Lett. **78**, 203 (1997).
[14] W. Just, D. Reckwerth, J. Möckel, E. Reibold, and H. Benner, Phys. Rev. Lett. **81**, 562 (1998).
[15] W. Just, in *Handbook of Chaos Control*, edited by H. G. Schuster (Wiley-VCH, Weinheim, 1999).
[16] W. Just, E. Reibold, H. Benner, K. Kacperski, P. Fronczak, and J. Holyst, Phys. Lett. A **81**, 158 (1999).
[17] H. Nakajima, Phys. Lett. A **232**, 207 (1997).
[18] W. L. Ditto, S. N. Rauseo, and M. L. Spano, Phys. Rev. Lett. **65**, 3211 (1990).
[19] D. W. Sukow, M. E. Bleich, D. J. Gauthier, and J. E. S. Socolar, Chaos **7**, 560 (1997).
[20] T. Pierre, G. Bonhomme, and A. Atipo, Phys. Rev. Lett. **76**, 2290 (1996).
[21] S. Bielawski, D. Derozier, and P. Glorieux, Phys. Rev. E **49**, R971 (1994).
[22] C. Simmendinger and O. Hess, Phys. Lett. A **216**, 97 (1996).
[23] S. Boccaletti, D. Maza, H. Mancini, R. Genesio, and F. T. Arecchi, Phys. Rev. Lett. **79**, 5246 (1997).
[24] V. S. Zykov, A. S. Mikhailov, and S. C. Müller, Phys. Rev. Lett. **78**, 3398 (1997).
[25] C. Lourenço and A. Babloyantz, Neural Comput. **6**, 1141 (1994).
[26] K. Hall, D. J. Christini, M. Tremblay, J. J. Collins, L. Glass, and J. Billete, Phys. Rev. Lett. **78**, 4518 (1997).
[27] E. Schöll and K. Pyragas, Europhys. Lett. **24**, 159 (1993).
[28] D. Reznik and E. Schöll, Z. Phys. B: Condens. Matter **91**, 309 (1993).
[29] D. P. Cooper and E. Schöll, Z. Naturforsch, Z. Naturforsch., A: Phys. Sci. **50a**, 117 (1995).
[30] A. Wacker and E. Schöll, Z. Phys. A **93**, 431 (1994).
[31] E. Schöll, *Nonequilibrium Phase Transitions in Semiconductors* (Springer, Berlin, 1987).
[32] *Nonlinear Dynamics and Pattern Formation in Semiconductors and Devices*, edited by F.-J. Niedernostheide (Springer, Berlin, 1995).
[33] F.-J. Niedernostheide, M. Kreimer, H.-J. Schulze, and H.-G. Purwins, Phys. Lett. A **180**, 113 (1993).
[34] E. Schöll, F.-J. Niedernostheide, J. Parisi, W. Prettl, and H. Purwins, in *Evolution of Spontaneous Structures in Dissipative Continuous Systems*, edited by F. H. Busse and S. C. Müller (Springer, Berlin, 1998), pp. 446–494.
[35] A. Wacker and E. Schöll, Semicond. Sci. Technol. **9**, 592 (1994).
[36] S. Bose, A. Wacker, and E. Schöll, Phys. Lett. A **195**, 144 (1994).
[37] F.-J. Niedernostheide, H. Schulze, S. Bose, A. Wacker, and E. Schöll, Phys. Rev. E **54**, 1253 (1996).
[38] R. Symanczyk, S. Gaelings, and D. Jäger, Phys. Lett. A **160**, 397 (1991).
[39] M. Meixner, P. Rodin, and E. Schöll, Phys. Rev. E **58**, 2796 (1998).
[40] M. Meixner, P. Rodin, and E. Schöll, Phys. Rev. E **58**, 5586 (1998).
[41] M. E. Bleich and J. E. S. Socolar, Phys. Lett. A **210**, 87 (1996).
[42] A. Kittel, J. Parisi, and K. Pyragas, Phys. Lett. A **198**, 433 (1995).
[43] H. G. Schuster, *Deterministic Chaos*, 2nd ed. (VCH Verlagsgesellschaft, Weinheim, 1988).
[44] A. Alekseev, S. Bose, P. Rodin, and E. Schöll, Phys. Rev. E **57**, 2640 (1998).
[45] S. Zoldi and H. Greenside, Phys. Rev. E **57**, R2511 (1998).